Material Investigation and Optical Limiting Properties of Carbon Nanotube and Nanoparticle Dispersions

Sean M. O'Flaherty,* Robert Murphy, Stephanie V. Hold, Martin Cadek, Jonathan N. Coleman, and Werner J. Blau

Materials Ireland Polymer Research Centre, Department of Physics, Trinity College Dublin, Dublin 2, Republic of Ireland

Received: October 1, 2002; In Final Form: December 5, 2002

The fabrication of a polymer and carbon nanostructure composite material is reported. A comprehensive material investigation of this stable dispersed system is presented. The fabrication technique and characterization steps are described where it was found that multiwalled carbon nanotubes and other clearly defined carbon nanostructures were stably dispersed in the polymer matrix. The properties of the material are investigated to characterize the carbon phases present. Experimental measurements of optical limiting of nanosecond laser pulses by a range of these composite materials in solution are reported. These composites were varied according to carbon nanostructure mass content. The experiments were performed using an open aperture *z*-scan apparatus with 6 ns Gaussian pulses at 532 nm from a frequency-doubled Q-switched Nd:YAG laser. Saturation of the optical limiting was reached at carbon nanostructure mass percentages in excess of 3.8%, relative to the polymer mass. Mechanistic implications of the optical limiting are investigated via angular dependent scattering measurements.

1. Introduction

Organic materials provide an attractive alternative to inorganic material for the construction of photonic devices to control the physical properties of optical beams for a wide range of important applications. The lack of appropriate nonlinear materials has been a significant barrier in the development of such devices. To this end, organic materials such as porphyrins,[1] dyes,[2] and phthalocyanines[3−8] have been studied for nonlinear absorption, or "optical limiting", applications. Optical limiters are materials that strongly attenuate intense optical beams while exhibiting high transmittance for low-intensity ambient light levels. They are of significant interest for the protection of human eyes, optical elements, or optical sensors from intense laser pulses, as well as having potential application in the field of optical switching. Optical limiters rely on an effective nonlinear response such as nonlinear absorption or scattering to dissipate the incident light as a function of its intensity, to allow only a reduced transmission to the target area being protected.

From the point of view of carbon nanostructures as optical limiters, carbon black, C_{60}, and carbon nanotubes,[9] both single-walled (SWNT) and multiwalled (MWNT), have been extensively investigated. Mansour et al.[10] concluded that the dominant nonlinearity leading to optical limiting in carbon black suspensions and carbon black deposited on glass was thermally induced scattering. It has been shown that C_{60} in solution[11−14] excited with high intensity at 532 and 1064 nm behaves as a reverse saturable absorber. Similar optical limiting studies of SWNTs and MWNTs in suspension have been reported. Vivien et al.[15−17] concluded that nonlinear scattering due to thermally induced solvent-bubble formation and sublimation of carbon nanotubes was the principal mechanism leading to optical limiting in carbon nanotube suspensions. Similar results for MWNT and carbon black suspensions from optical limiting and pump−probe experiments led Sun et al. to conclude that the limiting mechanism in MWNT suspensions was nonlinear scattering.[18,19] Riggs et al.[20] performed optical limiting experiments on suspended and solubilized full length and shortened SWNTs and MWNTs. They reported that the dominant optical limiting mechanism was nonlinear scattering for the suspended systems and nonlinear absorption for the solubilized systems. In each of these studies, however, a detailed investigation of material composition was not carried out from the point of view of MWNT or SWNT concentration or purity.

However despite these studies being of significant fundamental importance the use of carbon nanostructures in a practical optical limiting application would require some form of matrix to disperse the nanostructures and allow the fabrication of films, coatings, or suspensions of the matrix and nanotube composite material. Previously it has been shown that nanotubes can be held in suspension using the polymer poly(*m*-phenylenevinylene-*co*-2,5-dioctyloxy-*p*-phenylenevinylene) (PmPV). This procedure doubles as a purification technique to remove the impurities via sedimentation to form temporally stable, high-purity, polymer-stabilized MWNT dispersions.[21−23] This then allows techniques such as liquid-phase chemistry or solution spectroscopy to be applied. In addition, thin films can be cast by conventional processes such as spin coating for solid-state applications. These composite materials have been extensively investigated mechanically,[24] electrically,[25,26] and optically.[27−29] A comprehensive study of the optical limiting properties of these composite dispersions has been reported recently.[30] It was found that the cause of the nonlinear dissipation was almost certainly due to a combination of nonlinear absorption and scattering.

In this paper, a comprehensive material investigation and optical limiting application of a new temporally stable, dispersed polymer and carbon nanostructure composite system is pre-

* Corresponding Author. Tel: +353 1 608 1324. Fax: +353 1 6711759. E-mail: oflahers@tcd.ie.

10.1021/jp0271108 CCC: $25.00
Published on Web 01/04/2003

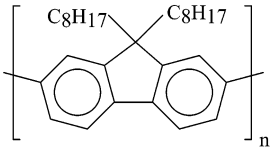

Figure 1. Repeat unit structure of the polymer poly(9,9-di-*n*-octylfluorenyl-2,7′-diyl), PFO.

sented. In this work the polymer used was the commercially available poly(9,9-di-*n*-octylfluorenyl-2,7′-diyl) (PFO). The fabrication technique and characterization steps are described where it was found that MWNT and other clearly defined carbon nanostructures were stably dispersed in the polymer. The properties of the material are investigated to characterize the carbon phases present. Furthermore the optical limiting is examined in relation to the ratio of the polymer to carbon nanostructure mass content in the dispersion and the possible mechanisms of the limiting are briefly discussed.

2. Experimental Section

2.1. Material Investigation. Soot containing carbon nanostructures was produced in our laboratory using the Krätschmer arc-discharge method.[31,32] In general, this soot is a multiphase system consisting of large-scale graphitic impurities and nanostructured materials such as multiwalled nanotubes (MWNTs) and multishelled nanoparticles. The nanotube content of this material has been measured as approximately 50% by mass.[32] It has previously been shown that composite formation using PmPV acts as a self-purifying system resulting in the stable dispersion of MWNTs and the sedimentation of all other graphitic species.[21,22] In this work, composite formation was investigated using the commercially available polymer, poly(9,9-di-*n*-octylfluorenyl-2,7′-diyl) (PFO) (Figure 1), which was obtained from the American Dye Source, Inc. (product code ADS129BE). To examine the dispersion properties of PFO, six identical samples were prepared, each with 60 mg of PFO added to 3 mL of toluene. Each of these was then heated at 50 °C for 30 min to dissolve the polymer. To each sample, 20 mg of nanotube soot was added and these composite mixtures were agitated for 1 min with a high-power sonic tip at 120 W. They were then agitated for an additional 2 h in a low-power (60 W) sonic bath to ensure complete and uniform dispersal. The composites were left to stand for different times varying from 0.5 to 96 h (in order to allow any impurities to fall out of solution). After this, each composite dispersion was decanted, leaving two phases: a black sediment and a suspension with a blue-black appearance. The sediments were then dried and weighed.

As previously reported, the nanotube content of a sample can be measured using electron paramagnetic resonance (EPR).[22,33,34] This is a resonance technique, which measures the microwave-induced transitions between electron spin energy levels ($m_s = +1/2$ and $m_s = -1/2$ for spin 1/2 systems), in the presence of a varying magnetic field for a fixed microwave frequency. Information about the environment of the unpaired electrons in a sample is contained in the g value, a characteristic number that differs according to the species present. For nanotubes $g = 2.012$,[35,36] whereas for graphitic impurities $g = 2.020$; and the resonance in both cases is attributed to conduction electrons.[36] This difference in g values corresponds to a difference in central magnetic field of about 15 G which allows the deconvolution of the signal into a nanotube and a non nanotube component as shown in Figure 2.

EPR was performed on the decanted suspension and sediment for each settling time. For each suspension, approximately 0.7 mL of the decanted solution was drop cast onto a spin-free quartz plate, after being briefly sonicated in the low-power sonic bath to ensure homogeneity. This produced solutes weighing about 15 mg each. In the case of the sediments, 2 EPR samples were prepared for each powder due to the fact that they were not fully homogeneous. Approximately 4.5 mg of sediment powder were placed in spin-free quartz tubes. By correct normalization,[33] the EPR signals for the solute and sediment could be directly compared, allowing the percentage of MWNTs and graphitic particles held in solution to be calculated for each sample.

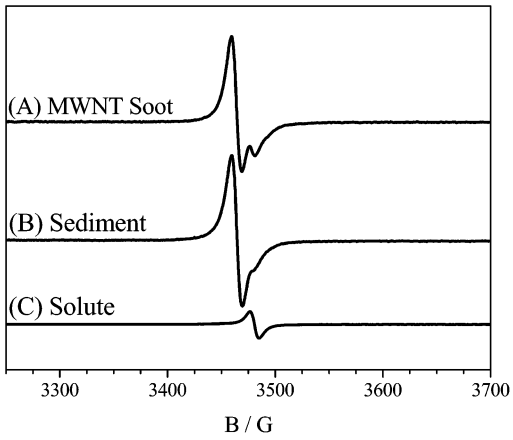

Figure 2. EPR derivative spectra of (A) original MWNT Krätschmer-generated soot, (B) the sediment from a typical PFO composite formed after 96 h settling time, and (C) a drop cast film made from the solute of a typical PFO composite formed after 96 h settling time.

2.2. Optical Experiments. After the above investigation a range of PFO−carbon nanostructure composite dispersions were prepared for optical application purposes. A 20 g L^{-1} solution of PFO in spectroscopic grade toluene was prepared. To this, a mass of arc-discharge soot equal to the mass of the PFO in solution was added. This was ultrasonically agitated using a high-power sonic tip over 40 s in order to accelerate the dispersion of the soot in the solution. The sample was then transferred to a low-power sonic bath where it was gently agitated for a number of hours. The solution was then left to stand undisturbed for 7 days. This was followed by the decantation of a stable dispersion of composite material in the form of a polymer host with carbon nanostructured inclusions in toluene. This suspension held the highest mass fraction of carbon nanostructures used in the optical experiments.

The mass of carbon nanostructure relative to PFO mass was varied in these samples by blending pure PFO in solution with the stable, decanted PFO−carbon nanostructure dispersion in the required ratios. The carbon nanostructure mass fraction in each sample was measured using thermogravimetric analysis (TGA). This involved measuring the mass of the sample as a function of temperature (from 25 to 1000 °C, at a constant heating rate of 10 °C/min). The gas used in all cases was air, with a flow rate of 20 L/min. These oxidation curves are plotted in Figure 3. It can be seen that by 700 °C the PFO sample is almost completely oxidized while the arc-discharge soot only begins to burn at temperatures just less than 800 °C. Similarly for the composite samples, almost no oxidation occurs between 700 °C and ∼780 °C. The stable mass in this region represents MWNTs and other carbon nanostructures. In Figure 3, normalized mass is plotted against the sample temperature. Numerical integration of the first derivative with respect to temperature over the carbon nanostructure section of the curve (720 °C − 970 °C) then gives the fractional mass of carbon nanostructures

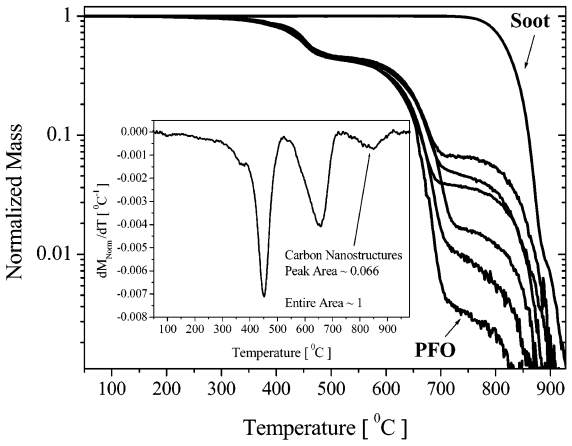

Figure 3. Thermogravimetric analysis (TGA) results for the PFO−carbon nanostructure composite materials used in the applications. The numerical integration of the respective peaks gives carbon nanostructure mass fractions, PFO = 0.000, 0.011, 0.019, 0.038, 0.050, and 0.066, and then pure soot.

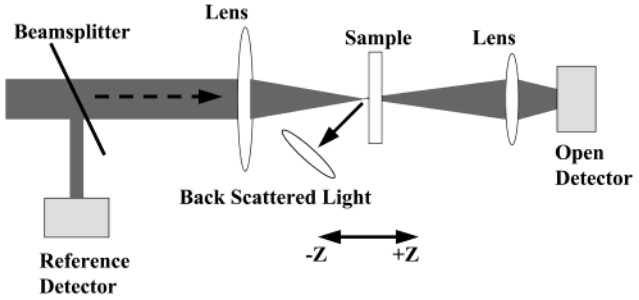

Figure 4. Schematic diagram of the experimental arrangement for the open aperture *z*-scan measurements. The arrow indicates the direction in which the backscattered light was measured.

present in the sample. The numerical integration over the entire curve gives a value of 1, the entire normalized mass. The inset is the first temperature derivative of the normalized mass for the composite with maximum carbon nanostructure content ≈ 6.6% as calculated from the numerical integration of the carbon nanostructure peak. Numerical integration of the other curves gave carbon nanostructure mass fractions of 0.011, 0.019, 0.038, 0.050, and 0.066 for the range of composite samples.

The open-aperture *z*-scan technique was employed to measure the total transmittance through the samples as a function of energy density for the optical limiting experiments.[37] The setup schematic is shown in Figure 4. All optical limiting experiments described in this study were performed using ~ 6 ns pulses from a Q-switched Nd:YAG laser. The beam was spatially filtered to remove higher order modes and tightly focused to approximately a 20 μm spot as determined from the open aperture spectra. The laser was operated at its second harmonic, 532 nm, with a pulse repetition rate of 10 Hz. All samples were measured in quartz cells with 1 mm path lengths at diluted concentrations of ≈1 g L^{-1}.

3. Results and Discussion

3.1. Material Characterization. The percentage of available nanotubes that remain suspended in the PFO solution after a particular settling time can be measured using EPR as described by Coleman et al.[33] By direct comparison of the signal intensities for the nanotube component in both the sediment and the solute, the percentage of nanotubes that are held in the PFO solution could be calculated for each settling time. Similarly, the percentage of non nanotube material held in the PFO solution

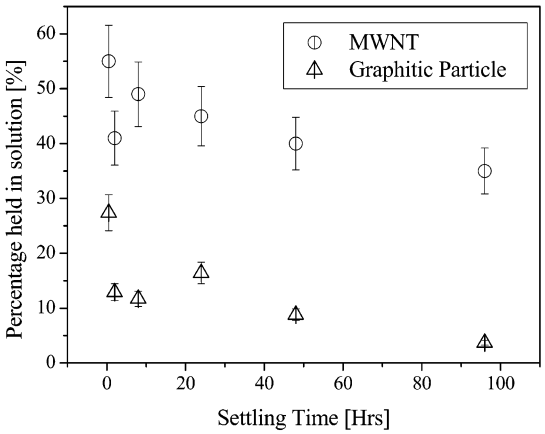

Figure 5. Percentage of MWNTs and graphitic particles (GP) held in solution (calculated using EPR) versus settling time.

was calculated in each case. These results are shown in Figure 5 as a function of settling time. It is quite apparent that the amount of non nanotube material held in solution falls dramatically over time, from 27% after 0.5 h to approximately 5% after 96 h. The nanotube dispersion however appears to be more stable, with the percentage of MWNT in solution falling from 55% after 0.5 h to 35% after 96 h. Additionally, after decantation the 96 h solution remained stable over a period of months with only minimal additional sediment forming. Thus PFO can be considered a suitable material for the stable dispersion of nanotubes.

However, this MWNT-PFO composite formation technique cannot be considered an efficient purification method for two reasons. First, after 96 h settling, over two-thirds of the nanotubes present had sedimented out of solution resulting in a rather low purification yield. In addition, combination of the EPR results with the TGA of the decanted solutes show that at least 10% by mass of the nonpolymer material in these purified samples consists of non nanotube carbon impurities. Transmission electron microscopy studies show that these carbon impurities are mainly in the form of nanoparticles, as shown in Figure 6. This compares with a maximum of 8% impurities observed for the PmPV-based composite purification method.[22] However TEM investigations show the non nanotube material in purified PmPV composites to be in the form of a small number of large-scale graphitic impurities. Conversely, the non nanotube material present in the PFO-based composite consists of a large number of well-defined nanoparticles. Thus the nanostructure component of the PFO composite consists of 90% by mass of MWNT and 10% by mass nanoparticles. If we assume that the average length and diameter of the MWNT used in this study are approximately 2 μm and 17 nm, respectively, and that the average diameter of the nanoparticles is similar to that of the nanotubes (as estimated from TEM) then it can be calculated that there are approximately 13 nanoparticles per nanotube in our stably dispersed composite materials. Thus, while the nanostructured material is mainly nanotubes, the number density of nanoparticles far exceeds that of the tubes.

The presence of large quantities of nanoparticles in the PFO-based composites can possibly be explained by the structure of PFO itself. The backbone of the PFO monomer consists of two six-membered rings connected by a pentagon. This is exactly the type of structure expected to provide the curvature needed for closure of graphitic nanoparticles. It has been shown previously that conjugated polymers tend to map onto the molecular structure of nanotubes.[38] It is therefore likely that the PFO backbone can bind efficiently to the graphitic nano-

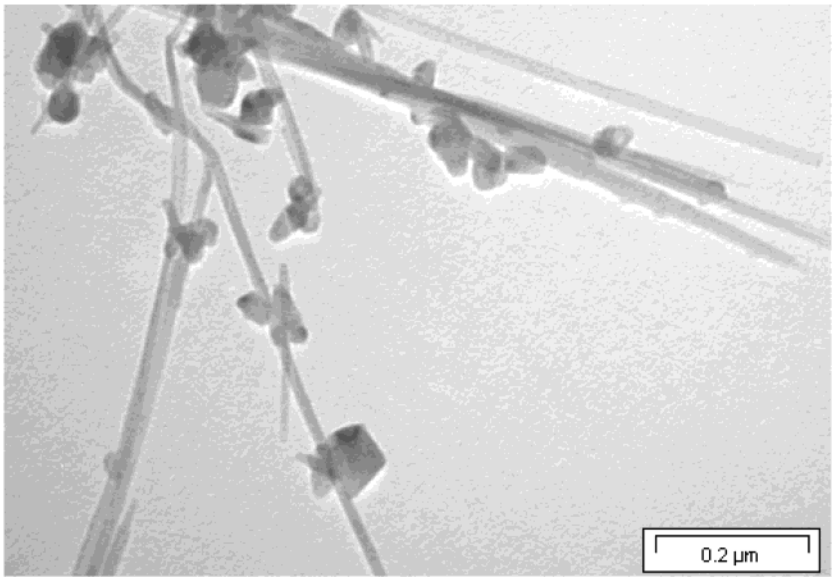

Figure 6. TEM of typical PFO and carbon nanostructure composite. In this image the polymer has been removed using Buchner filtration as described in ref 22. The nanotubes and graphitic particles can clearly be seen in the image.

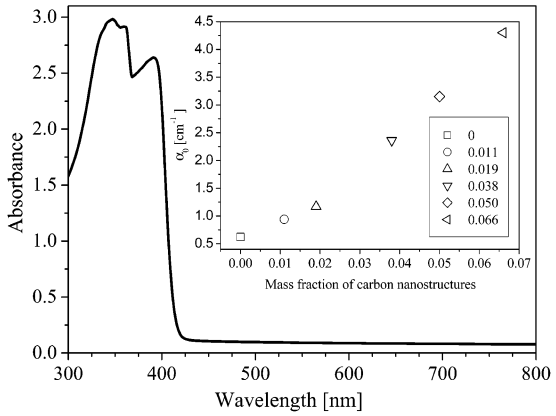

Figure 7. Typical visible spectrum for the PFO−carbon nanostructure materials. The inset plots the linear absorption coefficient against the carbon nanostructure mass fraction in the sample.

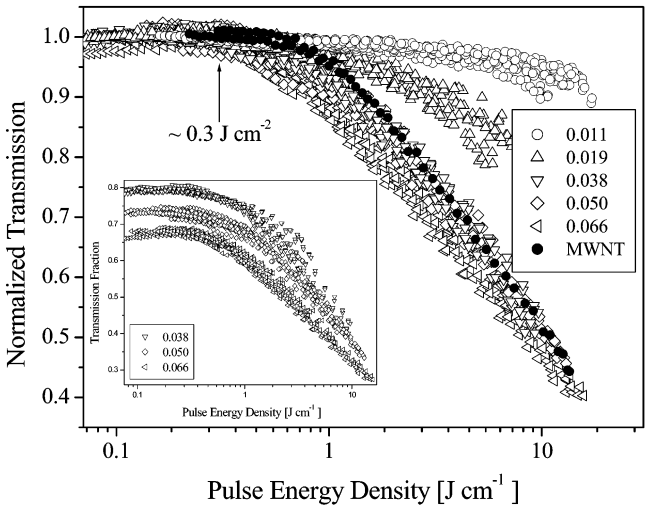

Figure 8. Plots of normalized transmission against incident pulse energy density for each sample. The data labeled MWNT is the optical limiting exhibited by a purified dispersion of multiwalled carbon nanotubes in toluene with linear transmission ≈ 67%. In the inset the samples with 0.038, 0.050, and 0.066 carbon nanostructure content are plotted as transmission against pulse energy density. The linear absorption is not normalized from the data in this case for clarity.

particles present in the crude soot, resulting in their dispersion in PFO-based composite solutions. Thus, these materials cannot be considered as polymer−nanotube composites in the strictest sense. However we can consider them as nanostructured carbon−polymer composites, which are interesting in their own right for optical applications.

3.2. Optical Characterization. The linear absorption spectra, recorded using a standard spectrophotometer at room temperature in the 200−1100 nm region, showed similar spectra for each of the composite dispersions. A representative spectrum from the composite dispersion with highest carbon nanostructure mass content is shown in Figure 7. The spectra for all samples were reasonably flat in the region of 532 nm with a relatively low linear absorption. The linear absorption coefficients at 532 nm for each of the composite dispersions are plotted against its carbon nanostructure mass fraction in the inset of the figure. As can be seen from this plot, the coefficients increase smoothly with the carbon nanostructure content. This was not unexpected, as successively increasing the relative volume of "black" particles to a partially transparent solution with a linear absorption coefficient = 0.62 cm^{-1} would obviously result in increasing that linear absorption coefficient.

The normalized nonlinear transmission plotted against incident pulse energy density for each of the samples measured using the open aperture *z*-scan technique can be seen in Figure 8. The pulse energy density is defined as $F_{\text{Pulse}} = E_{\text{Pulse}}/(\pi\omega(z)^2)$ in this case where E_{Pulse} is the energy in a single pulse, and $\omega(z)$ is the radius of the propagating Gaussian pulse as a function of position *z*. Several open aperture scans were taken for each sample with all scans superimposed on the same plot. In all cases the energy per pulse was increased in successive scans until the sample was damaged. For clarity, the transmission of the 0.038, 0.050, and 0.066 carbon nanostructure mass content samples were reproduced in the inset. In this case the data is not normalized and contains both its linear and nonlinear components. Data collected from a sample dispersion of purified multiwalled carbon nanotubes in toluene, labeled MWNT in the figure, with linear transmission of approximately 67% at 532 nm was also incorporated in the figure. This was added to allow comparison of the magnitude of the nonlinear response observed here with that of the response exhibited by other carbon nanostructure systems investigated by other authors. This linear

transmission percentage of the purified MWNT sample is approximately equal to the transmission of the composite with 0.066 carbon nanostructure mass content, which had a linear transmission ≈ 68%. The nanotubes were purified using the polymer PmPV and this purification method used to isolate MWNTs has been described recently.[22]

All samples containing carbon nanostructures show positive optical limiting about the focal point of the lens, while the pure polymer (carbon nanostructure mass fraction = 0.0) exhibits no dissipation of the incident light, regardless of the incident intensities. The pure PFO data has thus been omitted from the figure in the interest of clarity. The onset of optical limiting for the other samples is similar in all cases, and occurs approximately at ∼ 0.3 J cm^{-2}, indicating that the limiting is directly caused by the carbon nanostructures present in the composite dispersions. The limiting of the samples is mass fraction of carbon nanostructure dependent. The magnitude of the nonlinear effect increases systematically when the mass fraction of the nanostructures is increased from 0.011 to 0.038. The nonlinear effects, however, clearly become saturated at carbon nanostructure mass fractions in excess of ∼ 0.038. For example, at a pulse energy density of ∼ 8 J cm^{-2} the normalized transmission for the 0.011 nanostructure mass fraction sample is ≈ 94%, ≈ 80% for the 0.019 mass fraction sample, and ≈ 56%, 55%, and 53% for the remaining samples in order of increasing carbon nanostructure content. In all cases, data was collected for each sample up to the point at which the sample burned, which was ≈ 9.1 J cm^{-2}, ≈ 12.5 J cm^{2,} and ≈ 15.0 J cm^{-2} for the 0.038, 0.050, and 0.066 mass fraction of carbon nanostructures samples, respectively. It can be seen from the inset that the significant differences in the optical performance of the samples with nanostructure mass content 0.038, 0.050, and 0.066 are in the linear absorption regime (low energy density) and in the energy density above which the sample was damaged.

The origin of the interaction of the light with the composite materials has also been qualitatively investigated. The approach adopted involved measuring the scattered light from the samples, using a similar approach adopted by Mansour et al.[10] where simultaneous measurements of transmittance, absorbance, and scattering were made. The sample was placed on the focus of the *z*-scan focusing lens. The forward and backward scattered light (measured in arbitrary units) was simultaneously collected using additional lenses of diameter 6 cm with their axes at 45° to the *z*-axis of the experiment corresponding to a solid angle ≈ 1.05 steradian. The backscattering data is shown in Figure 9a and the front scattering data is shown in Figure 9b. Additional filters with 31% transmission were added to the front scattering detector, as this was the dominant scattering region. Similar results, with forward scattering intensity exceeding that of backscattering, have been reported for carbon black[10] and carbon nanotubes.[19] The backscattering signal exhibits a clear mass fraction of carbon nanostructure dependence. This contrasts with the front scattering (dominant scattering regime) data. The front scattering signal has saturated for the samples with the highest mass of carbon nanostructures. This is interesting when compared with the optical limiting data, which also appears to saturate at these carbon nanostructure mass fractions. The magnitude of the scattering signal for the 0.038 mass fraction sample is fractionally smaller, but approximately parallel, to the 0.050 and 0.066 mass fraction samples indicating that its scattering potential has also almost saturated. The angular dependence of the scattered light from the sample with maximum carbon nanostructure content (0.066 carbon nanostructure) was also measured and has been plotted in Figure 10, where the scattered signal in arbitrary units has been plotted as a function of angular position of the detecting diode. In this figure previously published scattering data from a PmPV and MWNT composite, with MWNT mass content ∼ 0.059, has been superimposed.[30] As mentioned above, the relative size of the front and backscattering lobes in Figure 10 for both the PFO

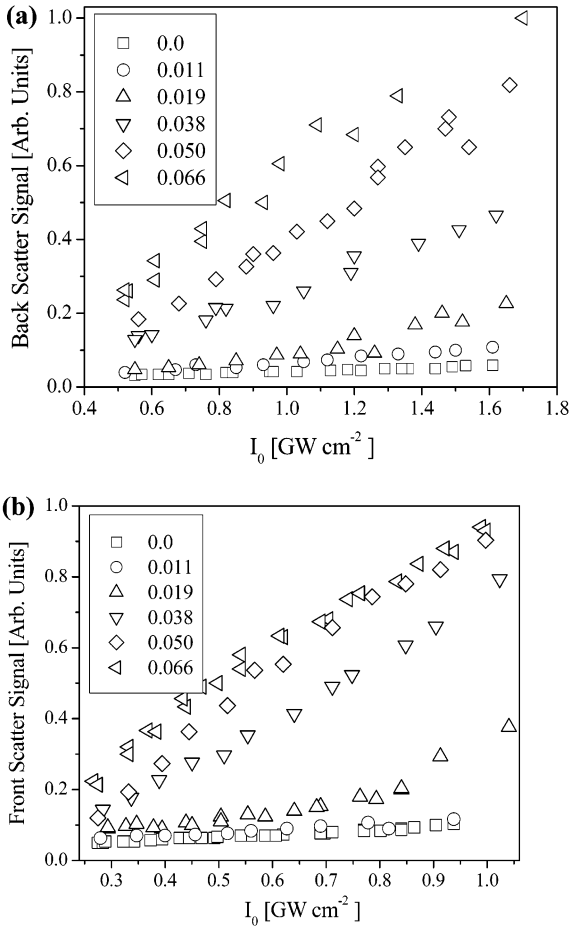

Figure 9. Plot of normalized backscattered light signal (a) and normalized front scattered light signal (b) as a function of incident intensity. The scattered light (measured in arbitrary normalized units) is collected using a lens of diameter 6 cm where the lens axis is at 45° to the *z*-axis and in the plane of the pulse corresponding to a solid angle ≈ 1.05 steradian. Additional filters with 23% transmission were added to the front scattering detector. The sample is positioned on focus of the *z*-scan lens.

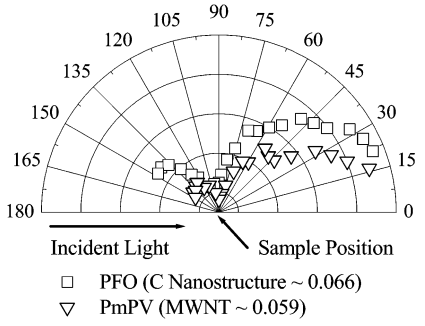

Figure 10. Polar plot of the scattered signal (arbitrary units) as a function of angular position of the detecting diode for a PFO and a PmPV-based composite sample. The plot displays the spatial distribution of the scattering lobes from the samples with carbon nanostructure mass content ≈ 6.6% in the PFO composite and with MWNT mass content ≈ 5.9% in the PmPV composite. The samples were irradiated at I_0 ≈ 1.7 GW cm^{-2} in both cases.

and PMPV-based composite dispersions is in qualitative agreement with the results quoted for carbon black[10] and MWNTs.[19] In these studies the cause of the scattering was reported to be due to thermally induced Mie scattering. It can be seen that there is a difference in the angular scattering profile of the PmPV and the PFO-based composite dispersions. In the PmPV composite the carbon nanostructure inclusions are almost exclusively MWNTs and accordingly Mie regime scattering with the front scattering lobe much larger than the backscattering lobe is observed. However, in PFO-based composite dispersions there are many spherical nanoparticles. Spherical particles with dimensions smaller than the wavelength of the incident light would be expected to exhibit Rayleigh scattering. Theoretically the angular profile of Rayleigh scattered light has front and backscattering lobes in equal proportions. Thus, in Figure 10 the PFO composite dispersion angular scattering profile is probably a linear sum of Mie scattering from the MWNTs and Rayleigh scattering from the spherical graphitic particles. This provides a logical explanation as to why the backscattering lobe is larger relative to the front scattering lobe for the PFO composite dispersion than for the PmPV composite dispersion.

4. Conclusion

In summary, a new composite material consisting of MWNT and multishelled graphitic particle inclusions stably dispersed in a commercially available polymer host (PFO) has been fabricated, materially investigated, and its optical limiting properties have been experimentally measured. In the composite material the carbon nanostructures were $\approx 90\%$ MWNTs by mass and the remainder were multishelled graphitic particles. It is likely that the PFO backbone can bind efficiently to the graphitic nanoparticles present in the crude soot, resulting in their dispersion in the composite. Thus, these materials cannot be considered as polymer−nanotube composites in the strictest sense as despite the nanostructured material being mainly nanotubes, the number density of nanoparticles far exceeds that of the tubes.

The higher carbon nanostructure mass fraction samples respond similarly when compared to other compounds currently being investigated for optical limiting applications, such as phthalocyanines[3−5] or naphthalocyanines.[39] These carbon nanostructure and polymer composite materials begin to dissipate light at similar pulse energy densities, and the magnitude of the dissipation is comparable with the most efficient of the reported compounds. These materials have the added advantage that embedding in a polymer host ensures that they are suitable for application to solid state without further modification.

The PFO-based composites clearly exhibit intensity-dependent scattering but there may also be other electronic absorption contributions to the optical limiting. Previously we have discussed the possibilities for excited-state absorption contributions to the optical limiting in poly(*m*-phenylenevinylene-*co*-2,5-dioctyloxy-*p*-phenylenevinylene) and MWNT dispersions.[30] It has been reported that electronic absorption in the form of multiphoton or excited-state absorption is possible from nanotubes.[29] The MWNT and spherical graphitic particle inclusions could also be differentiated in the scattering data. Rayleigh scattering contributions attributed to scattering from the spherical graphitic particles explain the difference in the angular profile of the scattering lobes in PmPV and the PFO-based composite dispersions. In the PmPV data exclusive Mie regime scattering was observed due to almost exclusive MWNT inclusions while the scattering from PFO-based composites is a combination of Rayleigh scattering from the spherical graphitic particles and Mie scattering from the MWNTs.

These composite systems are fabricated from commercially available raw materials. These types of materials also have the advantage that there is much potential for further optimization. It is possible that using single-walled nanotubes in place of MWNT could substantially reduce the mass fraction of nanotubes required for effective optical limiting. In addition, many potential host polymers remain to be tested. Future work will involve variation of both nanostructured guest and polymer host to improve dispersion properties and increase optical limiting efficiency toward real world applications.

Acknowledgment. S.O.F. and R.M. acknowledge Enterprise Ireland for financial support. The authors acknowledge the Irish Higher Education Authority (HEA), the European Union Network "COMELCAN", and the Electron Microscopy Unit, Trinity College Dublin.

References and Notes

(1) Henari, F. Z.; Blau, W. J.; Milgrom, L. R.; Yahioglu, G.; Phillips, D.; Lacey, J. A. *Chem. Phys. Lett.* **1997**, *267*, 229.

(2) Fakis, M.; Polyzos, J.; Tsigaridas, G.; Parthenios, J.; Fragos, A.; Giannetas, V.; Persephonis, P.; Mikroyannidis, J. *Chem. Phys. Lett.* **2000**, *323*, 111.

(3) Chen, Y.; Subramanian, L. R.; Fujitsuka, M.; Ito, O.; O'Flaherty, S.; Blau, W. J.; Schneider, T.; Dini, D.; Hanack, M. *Eur. J. Org. Chem.* **2002**, *8*, 4248

(4) O'Flaherty, S. M.; Hold, S. V.; Cook, M. J.; Torres, T.; Chen, Y.; Hanack, M.; Blau, W. J. *Adv. Mater.*, in press.

(5) Shirk, J. S.; Pong, R. G. S.; Flom, S. R.; Heckmann, H.; Hanack, M. *J. Phys. Chem. A* **2000**, *104*, 1438.

(6) Perry, J. W.; Mansour, K.; Lee, I. Y. S.; Wu, X. L.; Bedworth, P. V.; Chen, C. T.; Ng, D.; Marder, S. R.; Miles, P.; Wada, T.; Tian, M.; Sasabe, H. *Science* **1996**, *273*, 1533.

(7) Henari, F. Z.; Davey, A.; Blau, W.; Haisch, P.; Hanack, M. *J. Porphyrins Phthalocyanines* **1999**, *3*, 331.

(8) Hanack, M.; Schneider, T.; Barthel, M.; Shirk, J. S.; Flom, S. F.; Pong, R. G. S. *Coord. Chem. Rev.* **2001**, *219−221*, 235.

(9) Iijima, S. *Nature* **1991**, *354*, 56.

(10) Mansour, K.; Soileau, M. J.; Van Stryland, E. W. *J. Opt. Soc. Am. B* **1992**, *9*, 1100.

(11) Ganeev, R. A.; Ryasnyansky, A. I.; Kodirov, M. K.; Usmanov, T. *Opt. Commun.* **2000**, *185*, 473.

(12) Henari, F.; Callaghan, J.; Stiel, H.; Blau, W.; Cardin, D. J. *Chem. Phys. Lett.* **1992**, *199*, 144.

(13) McLean, D. G.; Sutherland, R. L.; Brant, M. C.; Brandelik, D. M.; Fleitz, P. A.; Pottenger, T. *Opt. Lett.* **1993**, *18*, 858.

(14) Barroso, J.; Costela, A.; Garcia-Moreno, I.; Saiz, J. L. *J. Phys. Chem. A* **1998**, *102*, 2527.

(15) Vivien, L.; Riehl, D.; Hache, F.; Anglaret, E. *J. Nonlinear Opt. Phys. Mater.* **2000**, *9*, 297.

(16) Vivien, L.; Anglaret, E.; Riehl, D.; Hache, F.; Bacou, F.; Andrieux, M.; Lafonta, F.; Journet, C.; Goze, C.; Brunet, M.; Bernier, P. *Opt. Commun.* **2000**, *174*, 271.

(17) Vivien, L.; Riehl, D.; Lancon, P.; Hache, F.; Anglaret, E. *Opt. Lett.* **2001**, *26*, 223.

(18) Sun, X.; Xiong, Y. N.; Chen, P.; Lin, J. Y.; Ji, W.; Lim, J. H.; Yang, S. S.; Hagan, D. J.; Van Stryland, E. W. *Appl. Opt.* **2000**, *39*, 1998.

(19) Sun, X.; Yu, R. Q.; Xu, G. Q.; Hor, T. S. A.; Ji, W. *Appl. Phys. Lett.* **1998**, *73*, 3632.

(20) Riggs, J. E.; Walker, D. B.; Carroll, D. L.; Sun, Y. P. *J. Phys. Chem. B* **2000**, *104*, 7071.

(21) Coleman, J. N.; Dalton, A. B.; Curran, S.; Rubio, A.; Davey, A. P.; Drury, A.; McCarthy, B.; Lahr, B.; Ajayan, P. M.; Roth, S.; Barklie, R. C.; Blau, W. J. *Adv. Mater.* **2000**, *12*, 213.

(22) Murphy, R.; Coleman, J. N.; Cadek, M.; McCarthy, B.; Bent, M.; Drury, A.; Barklie, R. C.; Blau, W. J. *J. Phys. Chem. B* **2002**, 106, 2210.

(23) Coleman, J. N.; Curran, S.; Dalton, A. B.; Davey, A. P.; Carthy, B. M.; Blau, W.; Barklie, R. C. *Synth. Metals* **1999**, *102*, 1174.

(24) Cadek, M.; Fougloc, B. L.; Coleman, J. N.; Barron, V.; Sandler, J.; Shaffer, M. S. P.; Fonseca, A.; Es, M. v.; Schulte, K.; Blau, W. J. *Kirchberg/Tirol, Austria, AIP Conference Proceedings* **2002**.

(25) Coleman, J. N.; Curran, S.; Dalton, A. B.; Davey, A. P.; McCarthy, B.; Blau, W.; Barklie, R. C. *Phys. Rev. B* **1998**, *58*, R7492.

(26) Fournet, P.; Coleman, J. N.; Lahr, B.; Drury, A.; Blau, W. J.; O'Brien, D. F.; Horhold, H. H. *J. Appl. Phys.* **2001**, *90*, 969.

(27) Dalton, A. B.; Byrne, H. J.; Coleman, J. N.; Curran, S.; Davey, A. P.; McCarthy, B.; Blau, W. *Synth. Met.* **1999**, *102*, 1176.

(28) Brennan, M.; Coleman, J. N.; in het Panhuis, M.; Kobayashi, T.; Blau, W. J. *Opt. Lett.*, in press.

(29) Brennan, M. E.; Coleman, J. N.; in het Panhuis, M.; Kobayashi, T.; Blau, W. J. *Proceedings of SPIE, Linear and Nonlinear Optics of Organic Materials* **2001**, *4461*, 56.

(30) O'Flaherty, S. M.; Hold, S. V.; Cadek, M.; Drury, A.; Coleman, J. N.; Blau, W. J. *J. Opt. Soc. Am. B*, in press.

(31) Kratschmer, W.; Lamb, L. D.; Fostiropoulos, K.; Huffman, D. R. *Nature* **1990**, *347*, 354.

(32) Cadek, M.; Murphy, R.; Carthy, B. M.; Drury, A.; Lahr, B.; Panhuis, M. i. h.; Coleman, J. N.; Barklie, R.; Blau, W. J. *Carbon* **2001**, *40*, *923*

(33) Coleman, J. N.; O'Brien, D. F.; Dalton, A. B.; McCarthy, B.; Lahr, B.; Barklie, R. C.; Blau, W. J. *J. Chem. Phys.* **2000**, *113*, 9788.

(34) Coleman, J. N.; O'Brien, D. F.; Dalton, A. B.; McCarthy, B.; Lahr, B.; Drury, A.; Barklie, R. C.; Blau, W. J. *Chem. Commun.* **2000**, 2001.

(35) Bandow, S. *J. Appl. Phys.* **1996**, *80*, 1020.

(36) Chauvet, O.; Forro, L.; Bacsa, W.; Ugarte, D.; Doudin, B.; Deheer, W. A. *Phys. Rev. B* **1995**, *52*, R6963.

(37) Sheik-Bahae, M.; Said, A. A.; Wei, T.-H.; Hagan, D. J.; Van Stryland, E. W. *IEEE J. Quantum Electron.* **1990**, *26*, 760.

(38) McCarthy, B.; Coleman, J. N.; Czerw, R.; Dalton, A. B.; Panhuis, M. i. h.; Maiti, A.; Drury, A.; Bernier, P.; Nagy, J.; Lahr, B.; Byrne, H. J.; Carroll, D. L.; Blau, W. J. *J. Phys. Chem. B* **2002**, *106*, 3087.

(39) Chen, Y.; O'Flaherty, S.; Fujitsuka, M.; Hanack, M.; Subramanian, L. R.; Ito, O.; Blau, W. J. *J. Chem. Mater.* **2002**, *14*, 5163.